Decoupling Mechanical and Interfacial Failure in Silicon Anodes via a Rigid-Flexible Binder Design for High-Energy-Density Lithium-Ion Batteries

Liuzhen Bian*[a,b,c], Zhaoxing Hu[a,b,c], Hongxiao Li[b,c,d], Xiaomei Zhang[a,b,c], Chaoyi Wang[b,c,d], Lei Xing[a,b,c], and Shengli An[b,c,d]

[a] School of Materials Science and Engineering, Inner Mongolia University of Science and Technology, Baotou, 014010, China

[b] Inner Mongolia Key Laboratory of Advanced Materials and Devices, Inner Mongolia University of Science and Technology, Baotou 014010, PR China

[c] Key Laboratory of Green Extraction & Efficient Utilization of Light Rare-Earth Resource (Inner Mongolia University of Science & Technology), Ministry of Education, Baotou 014010, PR China

[d] School of Rare Earth Industry, Inner Mongolia University of Science and Technology, Baotou 014010, China

Corresponding author: Liuzhen Bian: liuzhenbian@126.com;

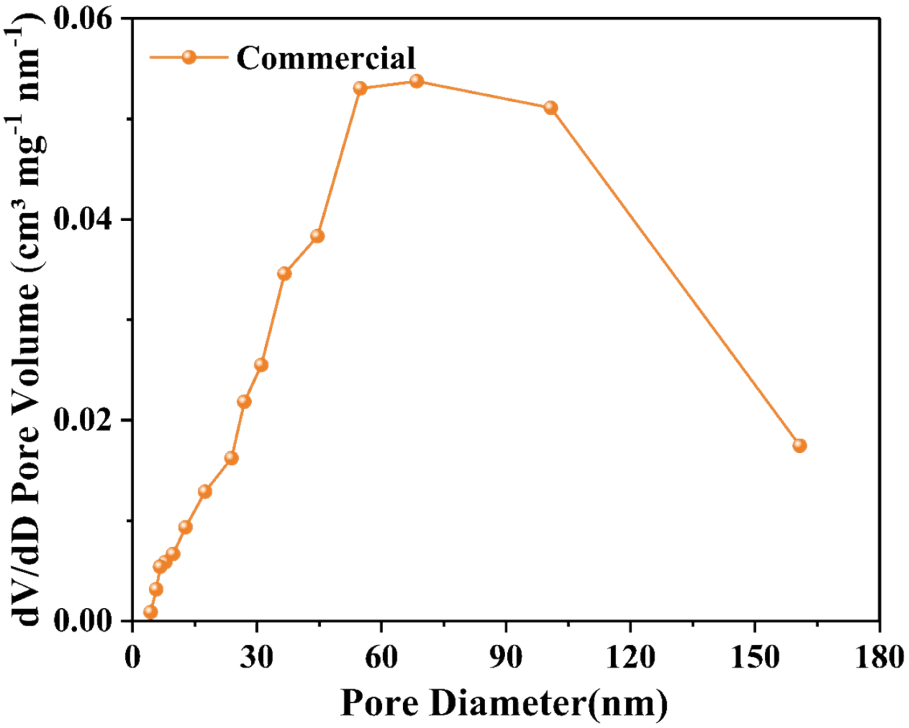

Fig. S1 Pore size distributions of pristine Si NPs.

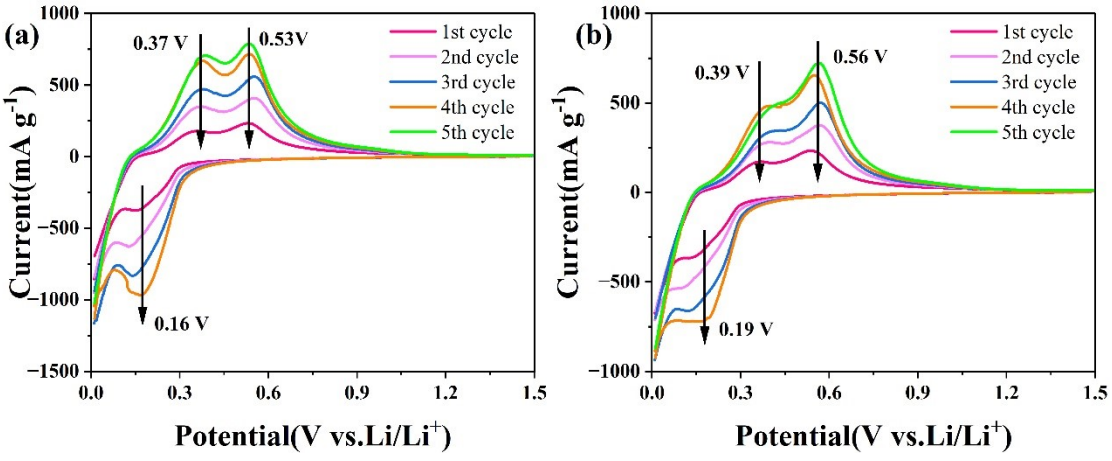

Fig. S2 (a) CV curves at 0.1 mV s^{-1} of Si-3:7 anode, (b) CV curves at 0.1 mV s^{-1} of Si-1:1 anode.

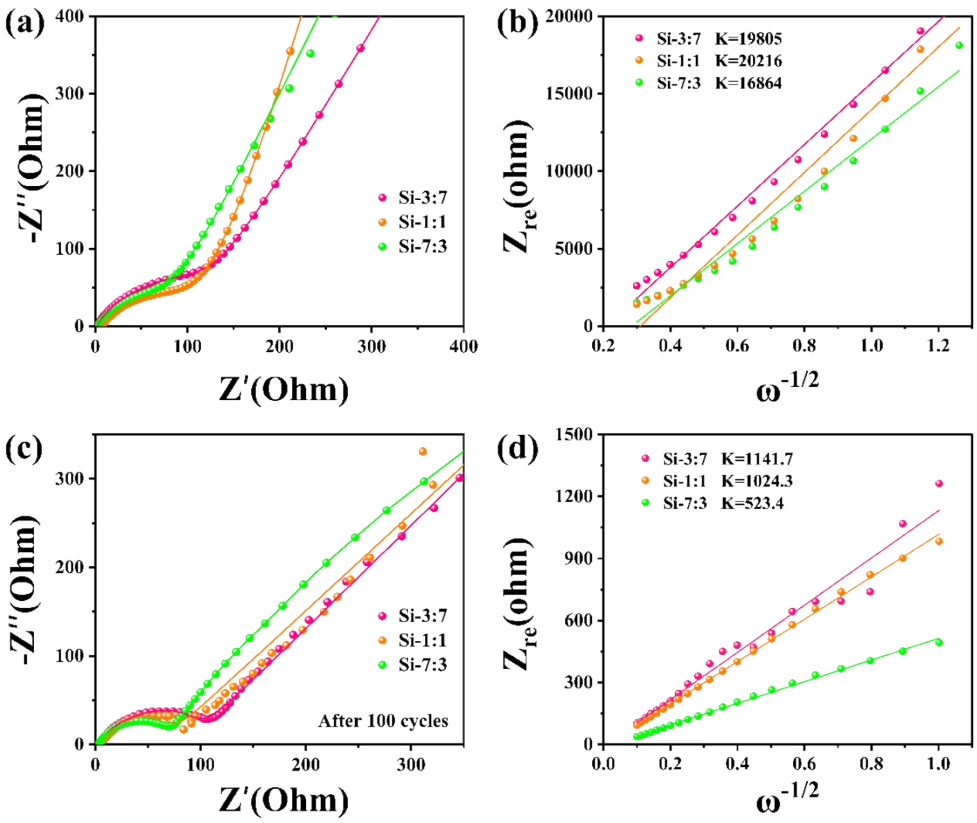

Fig. S3 Electrochemical impedance spectroscopy analysis of the Si-3:7, Si-1:1, and Si-7:3 electrodes. (a) Nyquist plots and (b) the linear relationship between Z_{re} and $\omega^{-\frac{1}{2}}$ in the low-frequency region before cycling. (c) Nyquist plots and (d) the corresponding linear fitting of Z_{re} and $\omega^{-\frac{1}{2}}$ after 100 cycles.

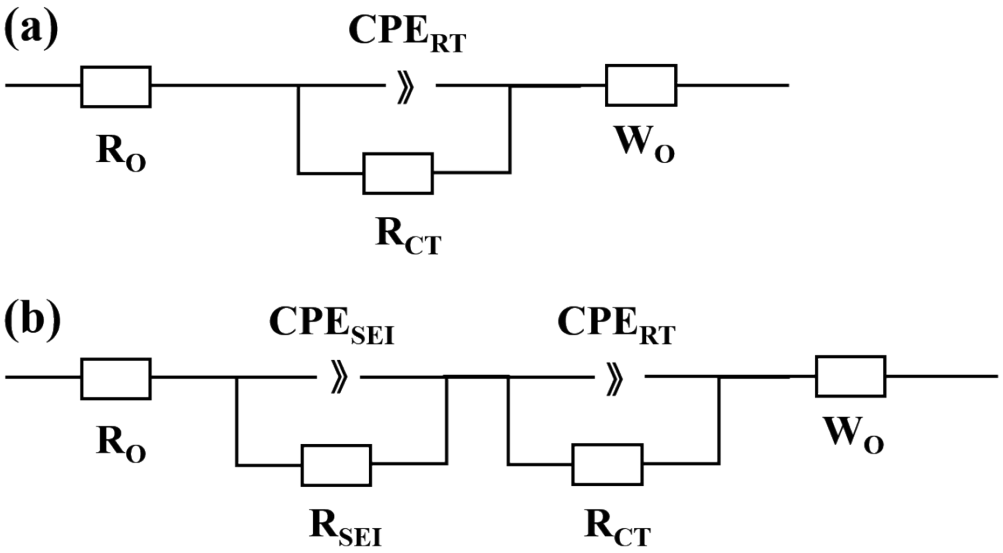

Fig. S4 (a) The analog circuit for Nyquist plots before cycling. (b) The analog b for Nyquist plots after cycling.

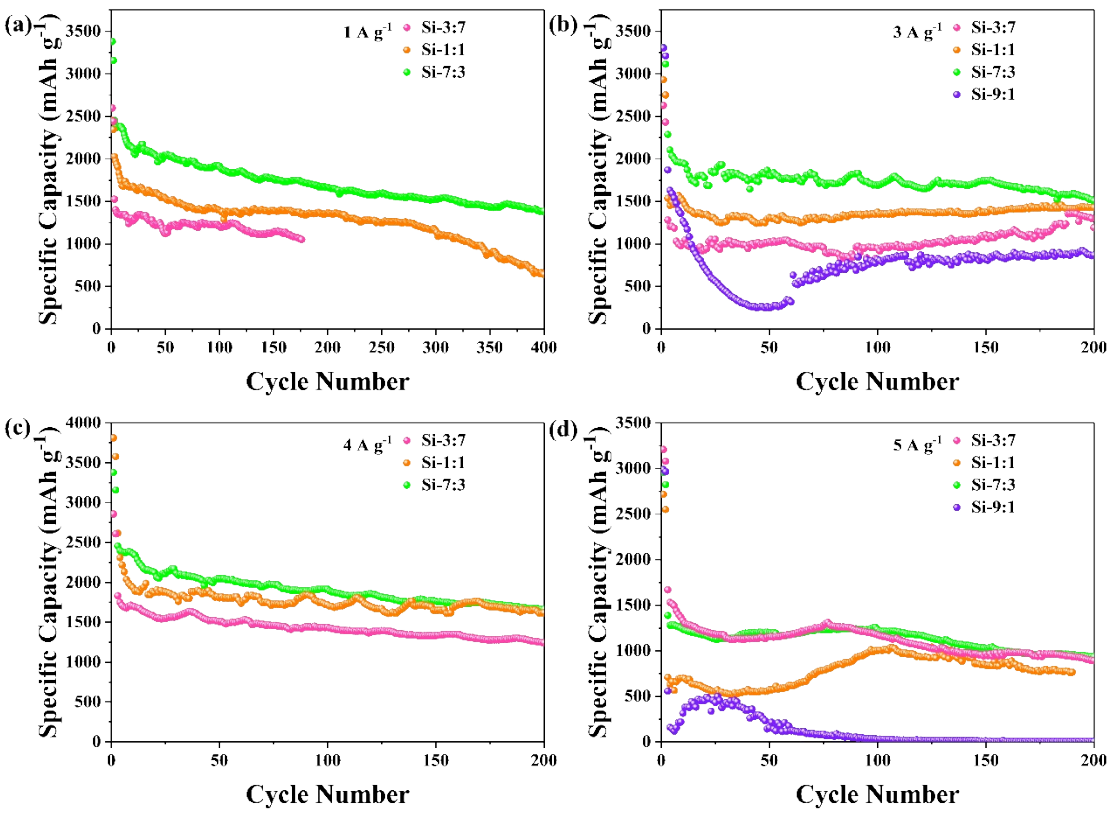

Fig. S5 (a-d) Cycling performances at 1A g^{-1}, 3A g^{-1}, 4A g^{-1} and 5A g^{-1} of Si-3:7, Si-1:1 , Si-7:3 and Si-9:1 anode.

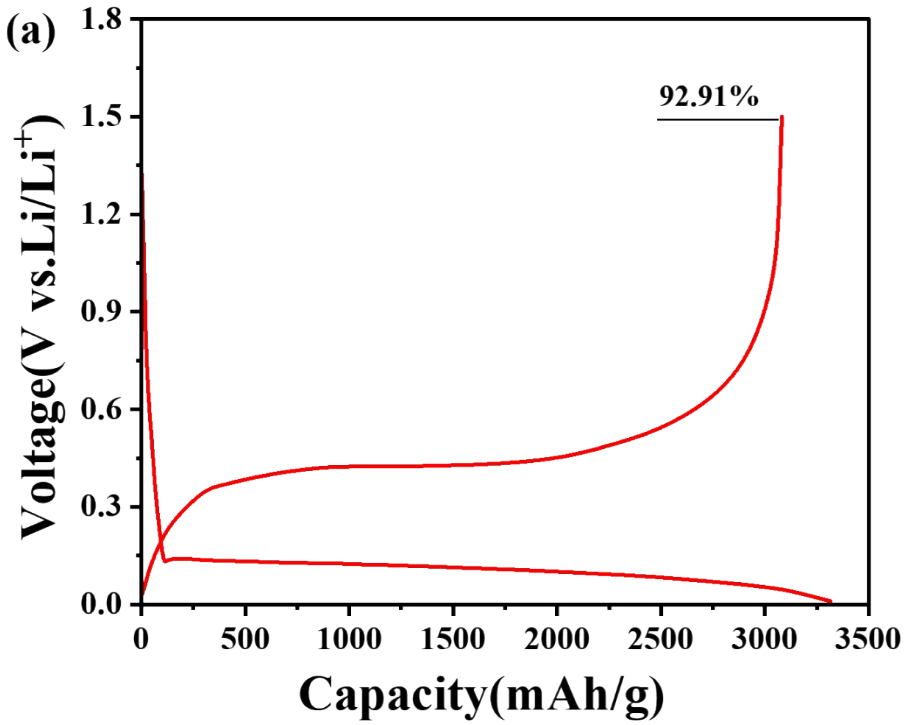

Fig. S6 (a) The initial charge–discharge curves of the Si-7:3 electrodes at 0.1A g^{-1}.

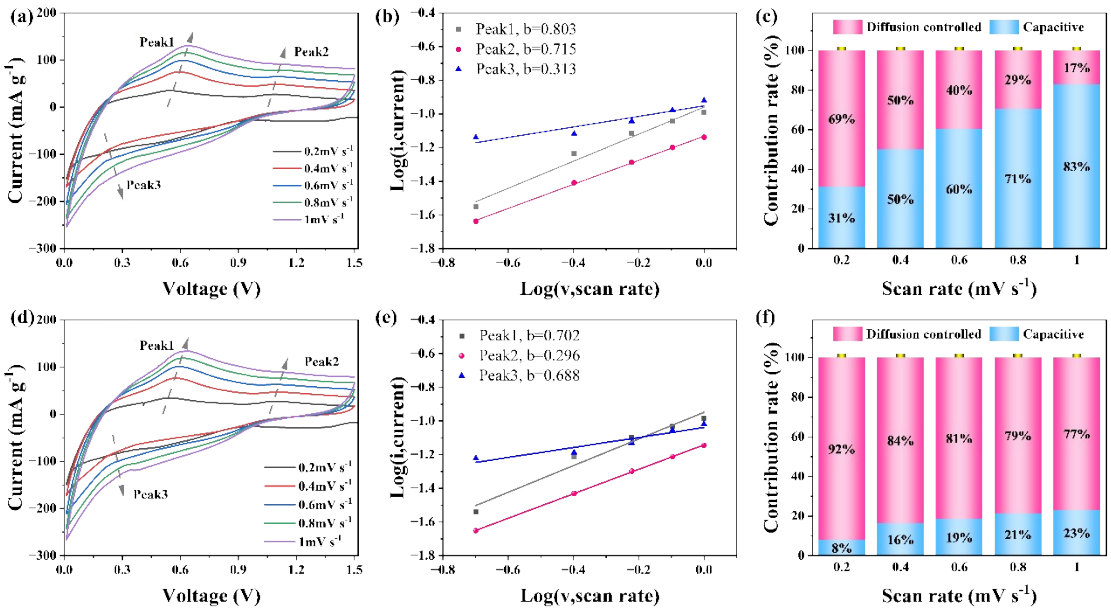

Fig. S7 (a, d) CV curves of Si-1:1, Si-3:7 electrode under different scan rates from 0.2 to 1.0 mV s^{-1}. (b, e) Corresponding plots of log(*i*) versus log(*v*) for the cathodic and anodic peaks. (c, f) Normalized contribution ratio of capacitive-controlled and diffusion-controlled processes at different scan rates for the Si-1:1 and Si-3:7.

Table S1 The peak area compositions of the C ls spectrum.

	Li_2CO_3	C=O	C-O	C-C	Total
Si-3:7	1.62%	11.59%	11.29%	75.5%	100%
Si-1:1	1.47%	11.76%	14.44%	72.33%	100%
Si-7:3	1.4%	11.21%	14.59%	72.8%	100%

Table S2. Detailed electrochemical conditions and performance metrics of the literature reports used for comparison in Fig. 4h, including cycle number, current density, and remaining specific capacity, together with the data from this work.

References	Cycle Number	Current density (A g^{-1})	Remaining specific capacity (mAh g^{-1})
Ref.S1	150	0.5	1000
Ref.S2	100	0.1	1250
Ref.S3	100	0.1	300
Ref.S4	200	0.2	230
Ref.S5	200	0.5	1500
Ref.S6	200	0.2	750
Ref.S7	100	1	900
Ref.S8	200	1	450
Ref.S9	200	0.5	520
Ref.S10	200	4	500
This work	200	2	1875.3

References

[S1] He, J, Ding, W, Xiao, L, et al. A dynamic boronic ester/hydrogen bonding enriched binder with self-healing chemistry for silicon anodes in lithium-ion batteries [J]. Chemical Engineering Journal, 2025, 518: 164454.

[S2] Yan, Z, Jin, H, Guo, J. Low-temperature synthesis of graphitic carbon-coated silicon anode materials [J]. CARBON ENERGY, 2019, 1(2) : 246-52.

[S3] Liu, Q, Ji, Y, Yin, X, et al. Magnesiothermic reduction improved route to high-yield synthesis of interconnected porous Si@C networks anode of lithium ions batteries [J]. ENERGY STORAGE MATERIALS, 2022, 46: 384-93.

[S4] An, Y, Tian, Y, Zhang, Y, et al. Two-Dimensional Silicon/Carbon from Commercial Alloy and CO_2 for Lithium Storage and Flexible $Ti_3C_2T_x$ MXene-Based Lithium-Metal Batteries [J]. ACS NANO, 2020, 14(12) : 17574-88.

[S5] Dai, S, Huang, F, Yan, J, et al. Construction of protein-like helical-entangled structure in lithium-ion silicon anode binders via helical recombination and hofmeister effect [J]. Advanced Science, 2025, 12(20) : 2412769.

[S6] Ma, K, He, Y, Zhao, X, et al. Lithium-ion battery silicon anodes: surface engineering with novel additives for enhanced ion and electron transport [J]. Chemical Engineering Journal, 2024, 496: 153846.

[S7] Chen, W, Li, W, Jiang, J, et al. Effect of binder types on performance of spherical and flaky silicon electrodes [J]. JOURNAL OF SOLID STATE ELECTROCHEMISTRY, 2024.

[S8] Chen, B, Xu, D, Chai, S, et al. Enhanced silicon anodes with robust SEI formation enabled by functional conductive binder [J]. Advanced Functional Materials, 2024, 34(34) : 2401794.

[S9] Zeng, X, Yue, H, Wu, J, et al. Hybrid Ionically Covalently Cross-Linked Network Binder for High-Performance Silicon Anodes in Lithium-Ion Batteries [J]. BATTERIES-BASEL, 2023, 9(5) : 276.

[S10] Zhang, W, Qian, M, Luo, G, et al. Improved lithium ion storage performance of $Ti_3C_2T_x$ MXene@S composite with carboxymethyl cellulose binder [J]. Journal of Colloid and Interface Science, 2023, 641: 15-25.